

This is the **accepted version** of the article:

Stribeck, Almut; Eling, Berend; Pöselt, Elmar; [et al.]. «Melting, Solidification, and Crystallization of a Thermoplastic Polyurethane as a Function of Hard Segment Content». *Macromolecular Chemistry and Physics*, Vol. 220, Issue 11 (June 2019), art. 1900074. DOI 10.1002/macp.201900074

This version is available at <https://ddd.uab.cat/record/204276>

under the terms of the  **CC BY** COPYRIGHT license

Melting, Solidification and Crystallization of a Thermoplastic Polyurethane as a Function of Hard Segment Content

Almut Stribeck^{a*}, Berend Eling^{a,c}, Elmar Pöselt^c, Marc Malfois^d,
Edgar Schander^c

^aInstitute of Technical and Macromolecular Chemistry, Bundesstr. 45, 20146 Hamburg, Germany.

Correspondence e-mail: almut@stribeck.de

^cBASF Polyurethanes GmbH, Elastogranstr. 60, 49448 Lemförde, Germany

^dALBA Synchrotron Light Source, 08290 Cerdanyola del Vallès, Catalonia, Spain

Abstract

Thermoplastic polyurethanes (TPU) with varying hard segment contents (HSC) are monitored during melting and solidifying ($|\dot{T}| = 20 \text{ K/min}$, $T_{max} = 220 \text{ °C}$) by small-angle and wide-angle X-ray scattering (WAXS and SAXS). Hard segments: MDI/BD. Soft segments: PTHF1000®. The neat materials are injection-molded having small amorphous hard domains (chord length $\bar{d}_h < 6 \text{ nm}$). Results indicate complexity of morphology changes. E.g. crystals are predominantly produced in freshly segregating, sufficiently big hard domains, while the temperature decreases slowly enough.

After the thermal treatment, only the materials with $\text{HSC} \gtrsim 35\%$ show sharp Bragg peaks and bigger hard domains ($\bar{d}_h > 7 \text{ nm}$). When heated, small domains melt, but crystallization in the remaining big domains is not detected. Upon cooling, first big agglomerates segregate, which crystallize immediately. Segregation starts for $\text{HSC} = 42\%$ at 160 °C and for $\text{HSC} = 75\%$ at 210 °C . When $\text{HSC} \leq 30\%$, the morphologies before and after are similar, but afterwards many hard blocks are dissolved in the soft phase on expense of the hard domain fraction. In heating and cooling the melts, we observe multiple homogenization and segregation processes, which are explained by agglomeration of hard blocks of different lengths in the colloidal fluid.

1 Introduction

The processes involved in melting and solidifying a thermoplastic polyurethane (TPU) are interpreted differently. It is clear that when solidifying hard blocks are stacked together and hard domains form. However, if and when hard domains become (semi)crystalline is explained differently

for many TPUs. As part of a systematic study of common TPUs, we now try to clarify how this question can be answered for an application-relevant class of TPUs that is at the center of our investigations. In these TPUs, the segments of their hard blocks (hard chain segments) consist of 4,4'-methylene diphenyl diisocyanate (MDI) and 1,4-butanediol (BD). BD is the chain extender. The soft segments are either polyesters or polyethers. Here we report on materials with different hard segment content (HSC), which have soft segments of the polyether polytetrahydrofuran (PTHF) with a molecular weight of 1000 (PTHF1000[®]).

In the literature there are many articles on the influence of the HSC on the properties of polyurethanes, including some that also study morphology. In 1982 Abouzahr et al. [1] investigate a series of TPUs that are very similar to ours, only the soft segments are twice as long. Their HSCs cover the range from 15 wt% to 45 wt%. The authors note that in the WAXS crystallization of the hard segments is not observed up to HSC = 35%. At HSC = 45% they observe crystallinity and an altered morphology. The domains are bigger and arranged so regularly that a distinct long-period peak arises. Our experiments support these findings.

Koberstein et al. [2] investigate a series of TPUs with HSCs ranging from 20% to 80%. For materials with an HSC below 40%, the small-angle X-ray scattering (SAXS) shows that the hard domains can not be lamellae. In the WAXS data crystallinity is found from an HSC of 40%.

Speckhard et al. [3] report increasing domain size with increasing HSC content. Garrett et al. [4] vary the HSC between 14% and 47%. They study their materials by atomic force microscopy and find that the domains in all materials are cylinders and spheres with dimensions in the order of 5-10 nm.

Swolfs et al. [5] study a TPU with a HSC=74% that is closely related to our materials (hard phase MDI/HD with the longer chain extender 1,6-hexanediol (HD)). They quench the material from the melt to the amorphous state and observe the morphology change on heating (low heating rate of 10 K / min) simultaneously with SAXS and WAXS. During the temperature increase, they observe weak cold crystallization and crystallization-induced phase separation. The phenomenon of cold crystallization [6, 7] is observed in the annealing of several polymers after quenching them from the melt to the amorphous state.

Briber and Thomas [8] are also studying a related TPU with an HSC of 77%. The hard phase is formed by MDI / BD. They highlight chain mobility as an important parameter of structure formation. A spherulitic structure is always found, but only the material produced with high chain mobility shows sharp Bragg reflections in the WAXS. The state of the corresponding hard phase they call "crystalline, type II". The low chain mobility material shows only diffuse WAXS peaks. Its hard phase is called "paracrystalline, type I". The study by Briber and Thomas builds a bridge to studies [9, 10] investigating crystallization and crystallography of the pure hard phase, i.e. polymeric MDI / BD.

Just as in the present study, we investigate in a recent study [11] TPU during melting and solidification in situ by SAXS and WAXS. In it we report that the morphology of the materials at high temperatures and moderate scan rate is dominated by unusual processes. As soon as the SAXS no longer detects hard domains at high temperatures, our TPUs are in the state of a colloidal melt, which generally changes its nature by mixing and demixing processes. This is suggested

by coupled modulations of SAXS and WAXS. In the case of ternary [12] or multiple segregation, several such modulations were observed.

In unpublished investigations under thermal load, we find no significant Bragg reflections in the WAXS for TPUs with a low hard segment content. Is this an indication that crystallization and crystallinity can often be neglected? To clarify this issue even in the case of mechanical load, some of us [13] have monitored the straining of four materials from the series of TPUs used here by SAXS and WAXS. In this study, the materials with HSC = 42% and 60% show a weak yet isotropic Bragg reflection already at low elongation. The TPUs with HSC \leq 30% show WAXS reflections only for strains $\varepsilon > 0.5$.

In the in-situ scattering experiments presented here, we focus on the conditions under which the mechanically unstressed material crystallizes, and are looking for answers to several questions. From which HSC do we observe crystallites in the neat material? Does crystallinity increase already in the heating branch (cold crystallization)? Does the material need to be melted before it crystallizes? Do amorphous and semi-crystalline materials have similar domain structure? How high is the crystallinity achieved as a function of the HSC?

2 Experimental Section

Materials. The studied thermoplastic polyurethanes are made by BASF Polyurethanes GmbH, Lemförde, Germany and consist of the same components. The hard segments are made from the diisocyanate 4,4'-methylene diphenyl diisocyanate (MDI) and from the chain extender 1,4-butanediol (BD). Soft segments are from the polyether polytetrahydrofuran (PTHF1000[®]).

Five materials of different composition have been made in the same way. They are characterized by their hard segment content (HSC), which ranges from HSC=22wt% to HSC=75wt% in the materials h22, h29, h42, h60 and h75. The numerical part of the labels indicates the HSC. For the production, PTHF and BD are weighed into a casting can and heated to 70 °C. At 60 °C, the MDI is added whilst stirring. The mixture is cast when the temperature of the mixture has reached 80 °C onto a hot plate of 80 °C. The slab remains on the hot plate for 10 min. The solidified materials are milled and injection-molded into sheets with dimensions 100 mm \times 100 mm \times 2 mm. The sheets are annealed at 80 °C for 15 h.

For comparison a similar TPU is investigated: H30 (“higher temperatures”) with a HSC = 30%. It consists of the same components, but is prepared in a slightly different process: The monomers are stirred at 80 °C, heated and cast at 110 °C. H30 is annealed at 100 °C for 20 h. It is the reference material from previous work [11], in which the same experimental technique has been used as in the present study. There and in a supplement the technique is presented in more detail.

Experimental technique sketched. Samples are heated at a constant heating rate $\dot{T} = 20$ K/min until $T_{max} = 220$ °C. They are kept at this temperature for 15 s and then cooled with $\dot{T} = -20$ K/min. Reported temperatures are rounded to the closest 5 °C. Experiments are carried out at beamline BL11-NCD of the Spanish synchrotron ALBA. SAXS and WAXS patterns are collected by two-

dimensional (2D) detectors with high spatial resolution. A notch in the WAXS detector allows to register more than 50% of the 2D WAXS image. SAXS and WAXS are registered with a frame rate of 3 s, corresponding to a temperature resolution of 1 K. The actual temperature of the sample in the irradiated volume may differ from the registered temperature.

3 Data Evaluation

3.1 Computing

Data are evaluated by the Python program SASKia (“small-angle scattering kit for interpretation and analysis”). The program source is free [14].

3.2 Preprocessing

Sample transmission. The background data $I_{2,b}(i)$ exhibit statistical noise of $\pm 10\%$. The raw transmission data $I_{2,f}(f)$, $f = 1 \dots 365$ during the experiments show similar noise. At low temperature the reading fluctuates about a constant value, and in the melt the smoothed $I_{2,f}(f)$ increases slowly. This is readily explained by the observed slight thinning of the irradiated region of the sample due to gravitational viscous flow. The curves $I_{2,b}(i)$ and $I_{2,f}(f)$ are smoothed yielding the value $\bar{I}_{2,b}$ and the curve $\bar{I}_{2,f}(f)$. Using the smoothed data avoids injection of the PIN-diode noise into the time line of the experiment. Consequently, the transmission coefficient c_t is approximated for each frame f by

$$c_t(f) \approx \frac{\bar{I}_{2,f}(f) I_{1,b}}{I_{1,f}(f) \bar{I}_{2,b}}. \quad (1)$$

Using the relation

$$c_t = \exp(-\mu t_m) \quad (2)$$

and the assumption that the linear absorption coefficient μ does not change during the experiment, the scattering of each frame is corrected for zero absorption and constant sample thickness t_m . The intensities are calibrated to absolute units using a polypropylene standard of known scattering power. Because of the variation of the colloidal nature of the materials we refrain from discussing the absolute values.

WAXS Data Preprocessing. Only the WAXS is affected by the diffraction from the aluminum wrapping. In the WAXS curve each aluminum spike appears twice, namely from each the front and the back foil of the sample wrapping. Thus the distance Δs_t between twinned aluminum peaks is a footprint of the unavoidable smearing of each wide-angle X-ray diffraction (WAXD) feature in the WAXS pattern. Consequently, a median filter of width $\Delta s_t/2$ applied to the curve removes all the Al-peaks without affecting possible diffraction peaks of the sample.

Background Subtraction. Finally, the recorded machine background is subtracted from each corrected frame.

3.3 Trend Visualizations

Curve of Total WAXS. If $I_{WAXS}(s)$ is the WAXS curve obtained so far, a convenient curve for further assessment is

$$I_{W,Q}(s) = 4\pi s^2 I_{WAXS}(s). \quad (3)$$

Here $s = (2/\lambda) \sin \theta$ is the modulus of the scattering vector with the scattering angle 2θ and λ the wavelength of the radiation. In the case of our TPUs this curve shows that the second order of the amorphous halo ends at $s_{h2} \approx 8 \text{ nm}^{-1}$. From the theoretical point of view the integral

$$Q_W = \int_0^\infty I_{W,Q}(s) ds \quad (4)$$

counts all the electrons which contribute to the WAXS [15–17] – if only the incoherent background c_C can be subtracted. Only to estimate if the WAXS is subjected to absorptive loss in the experiment, we approximate $c_C \approx I_{WAXS}(s_{h2})$ and obtain the representation

$$I_{W,total}(s) \approx 4\pi s^2 (I_{WAXS}(s) - I_{WAXS}(s_{h2})). \quad (5)$$

A more detailed explanation of this transformation and the following ones has been presented in previous work [11].

Visualization of the SAXS. Assuming elastic scattering, photons which are lost in the WAXS must show up in a different regime of scattering. In order to visually inspect, if some of such photons are found in the SAXS, a logarithmic representation of the SAXS intensity $I_{SAXS}(s)$ appears to be appropriate. It maps the intensity curve to a plot, in which changes at both ends of the SAXS curve easily catch the eye.

First, in $\log(I_{SAXS}(s))$ the high intensity blurring of the primary beam [18] becomes visible, which is typical for the multiple scattering in a colloid. In order to be able to record it, the SAXS detector must have a high dynamic range and also must detect at sufficiently small scattering angles.

Second, the logarithmic scaling enhances also variations of the background scattering in the tail of the SAXS, where the scattering is dominated by the density fluctuation scattering of the colloid. In order to record the fluctuation background, the SAXS detector must, additionally, be large.

3.4 Quantitative Analysis of the SAXS

General Concept. In analogy to previous work [11, 19–21] on TPU materials, the SAXS is analyzed quantitatively with respect to its information concerning the evolution of the two-phase morphology. The isotropic scattering curves are transformed into two fundamentally different real-space representations of the morphology, $g_1(r)$ and $g(r)$. A computation of Ruland’s interface

distribution function [22] (IDF) $g_1(r)$ from the isotropic SAXS is only reasonable, if the hard and the soft domains are lamellae. In the present studies this assumption leads to IDFs which are physically meaningless for the 3 samples with a low HSC (h22, h29, H30). Therefore, we generally analyze the morphology by means of chord distributions (CDs), which make no assumptions about the shape of the domains. CDs $g(r)$ after Méring and Tchoubar [23,24] only assume that the material can be approximated by two phases of different density. In our case these are the density of the domains and that of the matrix. All the measured CDs appear physically meaningful and fittable by the same short-range morphological model.

A CD is computed by projecting [25–27] the scattering curve $I(s)$ from 3D reciprocal space down to the 1D space by the Abel transform [28, 29] applied twice in succession. The resulting curve $\{I\}_1(s)$ is then multiplied by s^2 to reflect the 1D Porod law [30] of the real-space slice and converted into the interference function $G(s)$ by spatial frequency filtering [31]. Spatial frequency filtering is suitable for the processing of big data, because it runs automatically.

The Morphological Model for Fitting the Chord Distributions. The morphology of TPUs is very poor. It can be described by very simple structural models [11, 19–21, 32, 33], which at the most take into account correlations of hard domains with a next neighbor (“duo”). A second component considers such hard domains which are placed at random (“solo”). Only the duos make the SAXS long period (discrete scattering). The solo component takes into account excessive diffuse particle scattering, which can not be represented by the found discrete scattering. For the present melting-solidification studies, the most simple model of this class yields very good fits. It contains each one solo component and one duo component. In the model the two components are coupled by the restriction that the domain-size distribution of all domains is the same, regardless of whether a domain belongs to the solo component or to the duo component.

The fit returns the following parameters of physical meaning. $a(T) v_h$ is the product of the total volume filled by hard domains multiplied by a function $a(T)$ which is governed by the square of the contrast between hard-domain density and soft-domain density. $a(T)$ is supposed to increase with increasing temperature T . The supposition appears reasonable, if the thermal expansion coefficient α_s of the soft matrix is higher than the α_h of the hard domains. Thus at high temperature the returned value tends to overestimate the amount of remaining hard domains. In the case of the experiments reported here, the restriction may be less harsh: Anticipating the results, there is an indication that for $\text{HSC} \leq 35\%$ $\alpha_s \approx \alpha_h$ is valid and that for higher HSC the difference $|\alpha_h - \alpha_s|$ is monotonously increasing as a function of HSC. In analogy, $a(T) v_{duo}$ is an approximate measure of the volume fraction of the arranged domains which generate the SAXS long period. Related to the parameters directly defined in the model function, $a(T) v_h = (W_{solo} + W_{duo}) \bar{d}_h$ with W_i being the weight parameters of the fit [19, 21]. The “diameter” \bar{d}_h is, in fact, the number-average chord length [23, 34–36] of a hard domain. Similarly, \bar{d}_s is the average extension of the soft phase between a couple of arranged hard domains. Thus the number-average long period is $\bar{L} = \bar{d}_h + \bar{d}_s$. σ_h/\bar{d}_h is the relative standard deviation of the distribution of hard-domain diameters. In similar manner σ_s/\bar{d}_s quantifies the relative variation of the soft domain chords between two arranged hard domains.

Multi-Round Automated Fitting. A single experiment comprises 365 curves $g(r, f)$ with f symbolizing the frame index. In a first round of model fitting each curve is supplied with a standard set of starting parameters. This set is improved in three consecutive regression runs by the Simplex method [37]. As described in earlier work of one of us [31] the algorithm is extended by one step of the Levenberg-Marquardt algorithm in order to be able to assess the quality of the fit, as is described by Draper and Smith [38]. As a result, commonly only about 20% of the frames will have been fitted with excellent quality. So in the last step an automated algorithm supplies poorly fitted frames with appropriate starting values taken from the excellently fitted and runs fits over and over until most of the fits are excellent. A detailed description is in a previous paper [11].

4 Results and Discussion

4.1 Crystallinity and Related Morphology

Figure 1

[Figure 1 about here.]

combines scattering data with a presentation of the variation of the morphological parameters which are obtained by fitting the chord distributions $g(r)$. All the pseudo-color images are presented on the same “absolute” intensity scale. Remember, that doing so causes intensity-overflow in some images at ultra-small scattering angle. There a dark region means very high intensity, because the pseudo-color spectrum starts a second cycle. Let us describe what this scaling itself means. “Same scale” means that, first, in all the images the intensity zero is mapped to the color black and, second, the same intensity in units of e.u./nm⁶, i.e. “electrons per nanometer to the sixth” is mapped to the color white. Each sub-figure H30, h22-h75, is divided into 5 rows, “row a” to “row e”. Within each row the time propagates from left to right, and T_{max} is reached in the center.

Materials with HSC $\leq 30\%$. The sub-figures in the top of Figure 1 (H30, h22, h29) present the data of the materials with low HSC. The view of their SAXS (“row c”) gives a qualitative impression of the morphology evolution during the temperature cycle. Here the most prominent feature that varies is the long period peak. H30 and h29 share the same HSC, but H30 is processed at a higher temperature and annealed at 100 °C instead of 80 °C. In both materials the long period peak vanishes during heating at 185 °C and returns during cooling at 145 °C. The returning peak is diffuse in both cases. At 80 °C it broadens. The overall intensity of the discrete SAXS is higher for H30, the material that was prepared and annealed at the higher temperature. Also material h22 melts at 185 °C. On cooling the hard domain formation process appears blurred. Therefore, its onset temperature can not be determined reliably. In the central part of the time line all the materials are molten. Morphology variations in the molten states comprise mixing and segregation processes in a colloidal melt which are discussed in a separate section. In the solid state hard domains are present, but the WAXS of the low-HSC materials shows at best hints of a Bragg peak. Crystallinity appears to be negligible or very low.

Materials with HSC $\geq 42\%$. From h42 to h75, the melting temperature gradually increases. At the selected $T_{max} = 220$ °C the SAXS of h75 shows that it is not completely melted. That appears to be a reason why its WAXS shows no modulations due to the Tyndall effect [11]. All three materials start from a state in which the WAXS shows only indications of Bragg reflections. In the cooling branch, clear Bragg reflections are formed in the WAXS for all materials, even for h75. We suggest to identify the initial (Type I) and end states (Type II) with the two morphology designations suggested by Briber and Thomas [8]. According to these authors, Type I has paracrystalline hard domains that melt at $T_{m,I} = 207$ °C (\dot{T} not reported). Type I is formed when the TPU is solidified under restricted chain mobility. We can assume that the high cooling rate during injection molding of our TPUs has limited the chain mobility and prevented [5] crystallization. If solidification takes place under conditions of high chain mobility, Type II forms [5, 8] and sharp crystal reflections are observed – as in our samples after the thermal experiment. That may be due to the low scan rate $|\dot{T}|$ in our experiment. Crystals of Type II melt according to Briber and Thomas [8] at $T_{m,II} \approx 225$ °C. They report that their Type I material is not "recrystallized" by annealing at a T_{max} in the range $T_{m,I} < T_{max} < T_{m,II}$. However, we observe crystallization under this condition, but our in-situ experiment reveals that this is neither a cold [5] crystallization nor a recrystallization in the strict sense. Indeed, as Figure 1 ("row b") shows, the sharp Bragg peaks from h42 to h75 are formed only during the cooling phase in newly formed, big hard domains. Instead, typical for a cold crystallization would have been crystallization in the heating branch already at $T < T_{m,I}$. Crystallization in the heating branch would be termed "recrystallization", if it both occurred after exceeding $T_{m,I}$ and already Type I was assigned a certain order of molecular arrangement. In the big hard domains of h42 and h60 which persist at high temperature, we do not observe any crystallization, although their domain size corresponds to that of the domains which emerge newly on cooling and crystallize immediately. For h75, however, we can no longer exclude a slight increase in the sharp Bragg peaks already in the heating branch. So here cold crystallization may take place to a limited extent. At somewhat lower HSC the hard segments incorporated into amorphous hard domains do not appear to acquire the mobility necessary for crystallization until the domains are melted. If this finding proves to be universal, then this would be a major obstacle to the crystallization of the corresponding materials. What could be the reason for this inhibition of chain mobility in the old domains? The literature we found casts into doubt that persistent hydrogen bonds are the reason. This is the case, because several studies on polyurethanes report [39–43] that the hydrogen bonds in the hard domains dissociate already at low temperatures around 60 °C. Regarding the fraction of hydrogen bonds in the TPU, neither correlations with crystalline transitions within the hard domains [43] nor with the two-phase morphology [40] are observed. Only if the phase separation is improved, for example by annealing, the fraction of hydrogen bonds increases [43].

We are now trying to devise the conditions for a significant crystallization of the injection molded material. Significant crystallization only occurs on cooling, i.e. when the process is driven towards segregation ("pressure to segregate", $\dot{T}/|\dot{T}| = -1$). Furthermore, crystallization does not begin until the SAXS long period peak emerges (Figure 1, "row c"), which shows the formation of new hard domains, that is, when the segregation actually separates hard segments from soft

segments. As will be shown by the quantitative analysis of the SAXS, the crystallizing domains are bigger than the mean size of the amorphous domains of the neat material. In addition to the pressure to segregate, a certain minimum size of the domains may be necessary to allow crystallization.

Thus our experiments detect a complex sequence of mechanisms that lead to crystallization. If we add the findings from the literature cited in the introduction, the following conditions appear to be sufficient for our TPUs to crystallize:

1. A high HSC provides both a high hard-segment density and correspondingly hard blocks of sufficient length
2. Cooling of the material (pressure to segregate)
3. Low cooling rate (sufficient time), in order
 - (a) to generate hard domains of sufficient size (volume) by agglomeration of hard segments
 - (b) not to suppress the arrangement process of the still mobile hard segments.

If such strict conditions are even necessary for a temperature treatment aimed at significant crystallization of MDI/BD in injection molded TPU with $\text{HSC} \leq 70\%$, the requirements appear to be even more stringent than those for recrystallization or for a cold crystallization of typical polymers. The fact that we probably can not generalize our results for very high HSCs is shown both by the indication in h75 and a paper by Swolfs et al. [5]. They find cold crystallization at 120 °C with a similar TPU. Their TPU has $\text{HSC}=74\%$ and the longer chain extender 1,6-hexanediol (HD). Moreover, their heating rate is even lower as ours ($\dot{T} = 10 \text{ K/min}$). Even with these authors, the observed effect is weak. They write that “crystallinity is low and/or that the crystals themselves are small and/or of little internal order”.

Figure 1, “row b” shows that the most prominent crystalline reflections emerge with h60. We attribute this to the combination of an already relatively high HSC and a complete liquefaction of the material, which ensures sufficient chain mobility [5, 8].

The onset temperature at which the first sharp Bragg peaks are observed in the cooling branch at the cooling rate of 20 K/min is a function of the HSC. To start crystallization, h42 has to be cooled down to 160 °C, with h60 180 °C is sufficient, and with h75 the crystal reflections become noticeable already at 210 °C.

Let us now consider the course of the SAXS (Figure 1, “row c”). Similar to the low HSC materials, the position of the long-period peak does not change until warming to $\approx 110^\circ\text{C}$. On the other hand, the high-HSC TPUs in this temperature range exhibit a considerable increase of the long-period peak. Why does the peak intensity increase? An improvement in the phase separation as suggested by Swolfs et al. [5] is out of the question, because then the SAXS fluctuation background would have had to decrease significantly. Also other fingerprints are missing here, which could indicate change in the nature of the colloidal melt [11] necessary in a segregation process. Such fingerprints would be an increase of the multiple scattering in the SAXS and modulations of the WAXS by changing the strength of the Tyndall effect [11]. A possible explanation,

however, is an increase in contrast due to different thermal expansion coefficients of the soft and hard phases ($\alpha_h < \alpha_s$). because the SAXS intensity is proportional to the square of the contrast $\rho_h - \rho_s$ between the densities of hard and soft phase. This explanation would imply that $\alpha_h \approx \alpha_s$ holds for HSC $\leq 30\%$ and that for HSC $\geq 42\%$ the difference $|\alpha_h - \alpha_s|$ increases continuously with increasing HSC.

4.2 Domains in the Vicinity of the Molten State

In Figure 1 in each subfigure “row a” shows the variations of the domain volumes during the experiment. In the heating branch, a strong decrease of the total volume of hard domains (solid line) indicates melting. As already reported in a previous study [11], it is not the solo component but the duo component (dashed line) which survives in the melt. Thus, when passing into the melt, the density does not fluctuate statistically, but there remain undulations of density which even may lead to an increased value of $a(T) v_h$. Conversely, in the cooling branch the formation of stable hard domains is indicated by the solid line rising above the dashed line. The solid state can therefore be characterized in that the solid line $a(T) v_h$ extends above the dashed line $a(T) v_{duo}$ in each “row a” graph.

As also stated in the previous work [11], the curves in “row e” support this interpretation. “Row d” shows that in all materials the smaller hard domains melt earlier than the bigger ones.

Only h75 deviates from the common scheme, and this is explained by the fact that this material has such a high melting point that it is not molten but only annealed under the conditions of our experiment.

4.3 Colloidal Melt and Phase Separation

With all materials except h75 there is a high-temperature region in which all hard domains are molten. In this region we observe the modulation of the WAXD and the SAXS, which we described in detail in a previous article [11]. Our explanation is that in this temperature range the material is a colloidal melt whose colloidal character changes as a result of mixing and demixing processes. Demixing on a scale of a few nanometers leads to increased density fluctuations. In the SAXS they are manifested by higher background scattering. As the segregating regions grow big, multiple scattering occurs, which is observed at very small scattering angles in the SAXS. Both effects result in less photons being available to illuminate the WAXD (Tyndall effect [11]). Comparing the states of the materials before the experiment with the states afterwards exhibits that all melted materials afterwards show a significantly weaker intensity of the WAXS than before. The SAXS shows that this weakening is due to increased density fluctuations, so to a significantly poorer phase separation of the re-solidified material. Many photons are scattered by the "colloidal fog", that is, by the many impurities of the soft phase. Obviously there is so then a great potential to improve the phase separation by maturation or annealing. During such a treatment, the sunken hard-domain fraction could then also recover. Thus, the observed changes show that in the TPUs investigated a considerable proportion of the hard blocks can be dispersed in the soft phase. Whenever this

occurs, the volume fraction of the effective soft phase $v_{s,eff}$ must be significantly greater than $v_s = (1 - v_h) \approx (1 - \text{HSC})$. Therefore, we can not answer the question of when phase inversion (that is, $v_{s,eff} < v_{h,eff}$ with $v_{h,eff} + v_{s,eff} = 1$) occurs with rising HSC depending on the pretreatment. Anyway, it seems likely that still in the material h60 hard domains are dispersed in a soft matrix. In contrast, in h75, the curves of Figure 1, “row a” suggest that soft domains are dispersed in a hard phase matrix.

4.4 Crystals in Hard Domains

If crystals form in hard domains, then Bragg reflections resulting from diffraction (WAXD) are observed in the WAXS region. For the three low HSC materials, the WAXS region shows, at best, the faint hint of a crystal reflection. In contrast, for the high-HSC materials already the neat samples exhibit Bragg reflections which are more clear, but very weak.

For these materials Figure 2

[Figure 2 about here.]

presents the change of the WAXS curve shape by the melting/solidification experiment. The discussion of absolute changes appears to be irrelevant for our TPUs because of the WAXS modulations [11] due to the varying colloidal structure of the soft phase. With h42, in the cooling branch a weak crystal reflex becomes visible at $s = 2.2 \text{ nm}^{-1}$. With h60 and h75, several sharp crystal reflections are observed in the cooling branch (cf. also Figure 1). In the heating branch only very weak crystal reflections are discovered. Upon cooling, the first Bragg peaks appear along with the long-period peak of the SAXS. For all WAXS peaks on the first order of the amorphous halo, the final state then tunes in very quickly. As the analysis of the domain morphology will show, the formation of sharp crystal reflections is accompanied by a significant increase of the average hard domain size (average chord length [23,34]). The application of the temperature program leads only with h60 to Bragg peaks that rise well above the amorphous halo. The lower crystallinity of h75 appears as a result of incomplete melting.

Table 1

[Table 1 about here.]

lists for h60 the positions of the maxima of the clear Bragg peaks above the first order of the amorphous halo and compares these positions with the data found on single crystals from MDI/BD. The positions determined here each correspond to slightly smaller d -spacings than those reported in studies of single crystals [8,9,44]. This may be due to the shift of the reflex maximum of broad reflections by the transformation $I(s) \rightarrow s^2 I(s)$.

4.5 Changes of the Domain Morphology

The solid lines in the “rows a” of Figure 1 present the changes of the hard domain fractions. Solid hard domains are present, as long as the solid curve is above the dashed one. These temperature regions are the same regions in which the SAXS shows a long-period peak (“rows c”).

The highest hard domain fraction in the neat materials is found in h29 and H30. The corresponding fraction of h22 is lower by 25%, as is the HSC. Also, the high-HSC TPUs initially show lower hard domain fractions than the two materials with $\text{HSC} \approx 30\%$. This is remarkable and suggests for the high HSC materials that the unknown prefactor $a(T) \rightarrow a(T, \text{HSC})$ becomes also a function of the HSC itself. Variations of contrast, of the thermal expansion coefficients, and phase reversal that is not taken into account may cause this finding. A measure of the average size of the existing hard domains is their average chord length \bar{d}_h . It is displayed in the solid lines of “row d”. Correspondingly, the dashed lines show the course of the average chord lengths \bar{d}_s of the soft phase in the sandwich zone between two hard domains. For most materials, \bar{d}_s hardly changes during the experiment. This is to be expected, because the chain length of the soft segments is uniform. Only in the strongly crystallizing h60 does the fit show a strong increase of \bar{d}_s in the middle part of the cooling branch. We consider this an artifact resulting from the assumption that the simple morphology model of solos and duos adequately describes the material. This may be correct for the amorphous material, but that at the beginning of strong crystallization much more order is evoked, which cannot be described with meaningful parameter values of such a simple model. Nevertheless, even with h60, at the end of the experiment, a sufficiently distorted morphology is created, which appears suitable for the application of the simple model. So even for h60 we can compare the domain morphology of the neat materials with the corresponding morphologies after the experiment.

For the low-HSC materials, the temperature treatment does not alter the mean size \bar{d}_h of the hard domains nor the widths of the hard domain distributions (solid lines in “row e”). This is different with the high-HSC materials, which also crystallize. For h42 and h60 the average chord lengths \bar{d}_h have increased by 1 nm after the temperature treatment. Taking into account that at the end of the cooling phase, many small (amorphous) hard domains are generated which lower the average, this result appears to be significant. With h75, the experiment is nothing but annealing at high temperature close to the melting point. This character, which differs fundamentally from the melting-solidification experiment, explains both the doubling of \bar{d}_h observed here and the strong increase of the hard-domain fraction by improving the phase separation.

4.6 A Concept of TPU Crystallization

In summary and with some simplifications, we propose a concept of crystallization of our TPUs under the conditions of our experiment, which is sketched in Figure 3.

[Figure 3 about here.]

When injection molding $|\dot{T}|$ is very high and few amorphous hard domains are formed. During the subsequent annealing T_a is so low that the average size of the hard domains does not increase. However, the hard domain fraction increases strongly due to segregation from the impure soft phase. When melting with low $\dot{T} = 20 \text{ K/min}$ the small hard domains melt first. “Cold crystallization”, i.e. crystallization during heating is not observed — not even in big, high-temperature hard domains. Cooling with $\dot{T} = -20 \text{ K/min}$ results in the formation of new, big hard domains that crystallize

immediately. The onset temperature increases with increasing HSC. On further cooling, smaller, probably again amorphous hard domains arise, because then the chain mobility is probably no longer sufficient for a perfect arrangement of the hard segments.

In order not to complicate the cartoon, we have not outlined the mixing and segregation processes [11] occurring in the colloidal melt on many of our TPU materials.

5 Conclusions

We have been able to identify the presented relationships because we could study a well-graded series of TPU materials with optimal time resolution on a synchrotron beamline with well-concerted equipment. Such conditions are not yet common in materials science. In addition, it was necessary to automate the evaluation algorithms in order to fully analyze the large amount of data. We have chosen a common scan rate $|\dot{T}|$ and a common maximum temperature. Variation of these parameters would certainly bring more new knowledge.

A limit of $\text{HSC} \approx 35 \text{ wt\%}$ above which crystallization is observed is frequently described in the literature, and we confirm it for the studied injection molded materials. New beyond that appear our results on the dynamics of domain morphology evolution and crystallization. The degree of crystallinity reached in our melting-annealing experiments remains in the single-digit range rather than in the double-digit range. This statement is hardly due to a low sensitivity of the scattering method for low crystallinities, because sharp Bragg peaks in the cooling branch already occur together with the first new hard domains. We therefore assume that wide-angle X-ray scattering (WAXS) on our TPUs detects all crystallinity relevant to their material properties. Generally, the tested TPUs appear to be even less willing to crystallize than some amorphous homopolymers such as e.g. quenched polyethylene terephthalate (PET), which exhibits considerable cold crystallization above its glass transition temperature. This may become important not only as a rule of thumb. If other sources of crystallinity enhancement could be ruled out, one could, e.g., develop from this property a test of crystallizable engineering parts for exceeding the maximum service temperature. The results of our study also raise new questions. For example, it should be clarified whether the small amorphous hard domains generated at low $|\dot{T}|$ carry crystallization nuclei that break the barrier for cold crystallization. Moreover, it would be very interesting to monitor a quenching experiment to investigate in which temperature range domains of which size and which crystallinity arise. In the practical implementation of such an experiment, great difficulties are to be expected in seeking high quality data. On the other hand, basically feasible appears a study in which materials with different HSC are monitored with different [2] low scan rates in a calorimeter in the synchrotron beam while recording the SAXS and the WAXS simultaneously. Thus one could hopefully match multiple endotherms directly with morphological and colloidal transitions.

Acknowledgements. The experiments have been performed at beamline BL11 - NCD of ALBA Synchrotron with the collaboration of ALBA staff in the frame of project IH-2017072268, "Effect of nucleating agents on melting and solidification of thermoplastic polyurethanes". In particular

we have benefited greatly from the support of Juan Carlos Martínez and Eduardo Solano.

References

- [1] S. Abouzahr, G. L. Wilkes, Z. Ophir, *Polymer* **1982**, *23*, 1077.
- [2] J. T. Koberstein, A. F. Galambos, L. M. Leung, *Macromolecules* **1992**, *25*, 6195.
- [3] T. A. Speckhard, K. K. S. Hwang, S. L. Cooper, V. S. C. Chang, J. P. Kennedy, *Polymer* **1985**, *26*, 70.
- [4] J. T. Garrett, C. A. Siedlecki, J. Runt, *Macromolecules* **2001**, *34*, 7066.
- [5] Y. Swolfs, E. Bertels, I. Verpoest, B. Goderis, *Polymer* **2015**, *81*, 1.
- [6] B. Wunderlich, *J. Chem. Phys.* **1958**, *29*, 1395.
- [7] B. S. Hsiao, K. H. Gardner, D. Q. Wu, B. Chu, *Polymer* **1993**, *34*, 3996.
- [8] R. M. Briber, E. L. Thomas, *J. Macromol. Sci. Part B: Physics* **1983**, *22*, 509.
- [9] L. Born, J. Crone, H. Hespe, E. H. Müller, K. J. Wolf, *J. Polym. Sci. Part B: Polym. Phys.* **1984**, *22*, 163.
- [10] J. Blackwell, C. D. Lee, *J. Polym. Sci. Part B: Polym. Phys.* **1984**, *22*, 759.
- [11] A. Stribeck, R. Dabbous, B. Eling, E. Pösel, M. Malfois, E. Schander, *Polymer* **2018**, *153*, 565.
- [12] A. Fortini, R. P. Sear, *Langmuir* **2017**, *33*, 4796.
- [13] X. Li, Y. Lu, H. Wang, E. Pösel, B. Eling, Y. Men, *Eur. Polym. J.* **2017**, *97*, 423.
- [14] A. Stribeck, “SASkia - a computer program for small-angle scattering analysis”, www.stribeck.de/saskia, **2018**.
- [15] A. Guinier, *X-Ray Diffraction*, Freeman, San Francisco, **1963**.
- [16] L. E. Alexander, *X-Ray Diffraction Methods in Polymer Science*, Wiley, New York, **1979**.
- [17] B. E. Warren, *X-Ray Diffraction*, Dover, New York, **1990**.
- [18] R. Perret, W. Ruland, *J. Appl. Cryst.* **1971**, *4*, 444.
- [19] A. Stribeck, X. Li, A. Zeinolebadi, E. Pösel, B. Eling, S. Funari, *Macromol. Chem. Phys.* **2015**, *216*, 2318.
- [20] X. Li, A. Stribeck, I. Schulz, E. Pösel, B. Eling, A. Hoell, *Eur. Polym. J.* **2016**, *81*, 569.
- [21] A. Stribeck, E. Pösel, B. Eling, F. Jokari-Sheshdeh, A. Hoell, *Eur. Polym. J.* **2017**, *94*, 340.
- [22] W. Ruland, *Colloid Polym. Sci.* **1977**, *255*, 417.
- [23] J. Méring, D. Tchoubar, *J. Appl. Cryst.* **1968**, *1*, 153.
- [24] D. Tchoubar, J. Méring, *J. Appl. Cryst.* **1969**, *2*, 128.
- [25] R. Bonart, *Kolloid Z. u. Z. Polymere* **1966**, *211*, 14.
- [26] H. Meyer, R. Bonart, *Progr. Colloid Polym. Sci.* **1985**, *71*, 103.
- [27] N. Stribeck, *X-Ray Scattering of Soft Matter*, Springer, Heidelberg, New York, **2007**.
- [28] N. H. Abel, *J. Reine Angew. Math.* **1826**, *1*, 153.
- [29] R. N. Bracewell, *The Fourier Transform and its Applications*, McGraw-Hill, Boston, 3rd edition, **1999**.
- [30] G. Porod, *Colloid Polym. Sci.* **1951**, *124*, 83.

- [31] N. Stribeck, *Colloid Polym. Sci.* **2002**, 280, 254.
- [32] N. Stribeck, A. Zeinolebadi, M. Ganjaee Sari, A. Frick, M. Mikoszek, S. Botta, *Macromol. Chem. Phys.* **2011**, 212, 2234.
- [33] N. Stribeck, A. Zeinolebadi, F. Harpen, G. A. Luinstra, B. Eling, S. Botta, *Macromolecules* **2013**, 46, 4041.
- [34] J. Méring, D. Tchoubar-Vallat, *C. R. Acad. Sc. Paris* **1965**, 261, 3096.
- [35] J. Méring, D. Tchoubar, C. Schiller, *Bull. Soc. fr. Mineral. Cristallogr.* **1967**, XC, 436.
- [36] G. Porod, in: R. R. Rowell, R. S. Stein, Eds. "Electromagnetic Scattering. Proceedings of ICES 2, Amherst, MA, June 1965", Gordon & Breach, New York, **1967** pp. 319–337.
- [37] M. S. Caceci, W. P. Cacheris, *Byte* **1984**, 1984, 340.
- [38] N. R. Draper, H. Smith, *Applied Regression Analysis*, John Wiley & Sons, New York, 2nd edition, **1980**.
- [39] R. W. Seymour, S. L. Cooper, *Macromolecules* **1973**, 6, 48.
- [40] C. S. Paik Sung, N. S. Schneider, *Macromolecules* **1977**, 10, 452.
- [41] V. W. Srichatrapimuk, S. L. Cooper, *J. Macromol. Sci. Part B Phys.* **1978**, 15, 267.
- [42] C. M. Brunette, S. L. Hsu, W. J. MacKnight, *Macromolecules* **1982**, 15, 71.
- [43] J. T. Koberstein, I. Gancarz, T. C. Clarke, *J. Polym. Sci. Part B: Polym. Phys.* **1986**, 24, 2487.
- [44] J. Blackwell, M. Ross, *J. Polym. Sci. Polym. Lett.* **1979**, 17, 447.

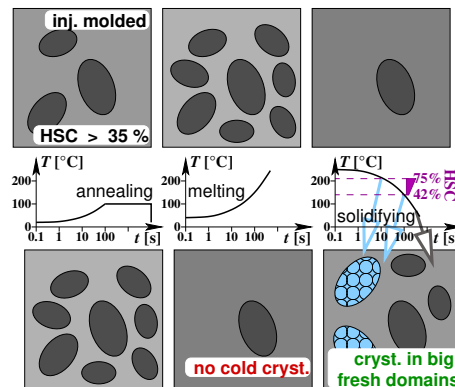
Melting, Solidification and Crystallization of a Thermoplastic Polyurethane as a Function of Hard Segment Content

Almut Stribeck, Berend Eling, Elmar Pöselt, Marc Malfois, Edgar Schander

Text for the Table of Contents

Simultaneous SAXS and WAXS indicate that crystals are predominantly produced for hard segment contents $HSC > 35\%$ in freshly segregating, sufficiently big hard domains, while the temperature decreases slowly enough. For lower HSC the thermal expansion coefficients of hard and soft phase appear to be similar.

Graphic for the Abstract and the Table of Contents



KEYWORDS: polyurethane; hard-segment content; microstructure; crystallization; scattering;

List of Figures

1	Melting and solidification of TPUs with varying hard segment content (HSC) as a function of processing temperature. Samples are heated and cooled with $ \dot{T} = 20\text{K/min}$, $T_{max} = 220^\circ\text{C}$, 15 s dwell-time at T_{max} . Presented are scattering data and results of morphology analysis. H30 : Hot processing, HSC = 30 wt%. — Cooler processing: h22, h29, h42, h60, h75 . Numbers indicate the HSC. a : volume fractions of hard domains. b : Total WAXS intensity curves $I_{W,total}(s)$, $1 < s < 8\text{nm}^{-1}$. c : SAXS $\log(I(s))$, $0 < s < 0.25\text{nm}^{-1}$. d : average domain diameters. e : widths of the domain-size distributions characterized by their relative standard deviations (Subfigure H30 from previous work [11])	18
2	Before and after the temperature cycle. Comparison of the curve shapes of the total WAXS intensities, $s^2I(s)$, for the materials with $\text{HSC} \geq 42\text{ wt\%}$. Dashed lines: neat materials. Solid lines: After the temperature treatment. HSC is the numerical part of the label.	19
3	The dominant effects of hard-domain evolution and crystallization at the thermal processing steps of crystallizable TPU materials from the present investigation. Segregation processes within the colloidal melt are not sketched	20

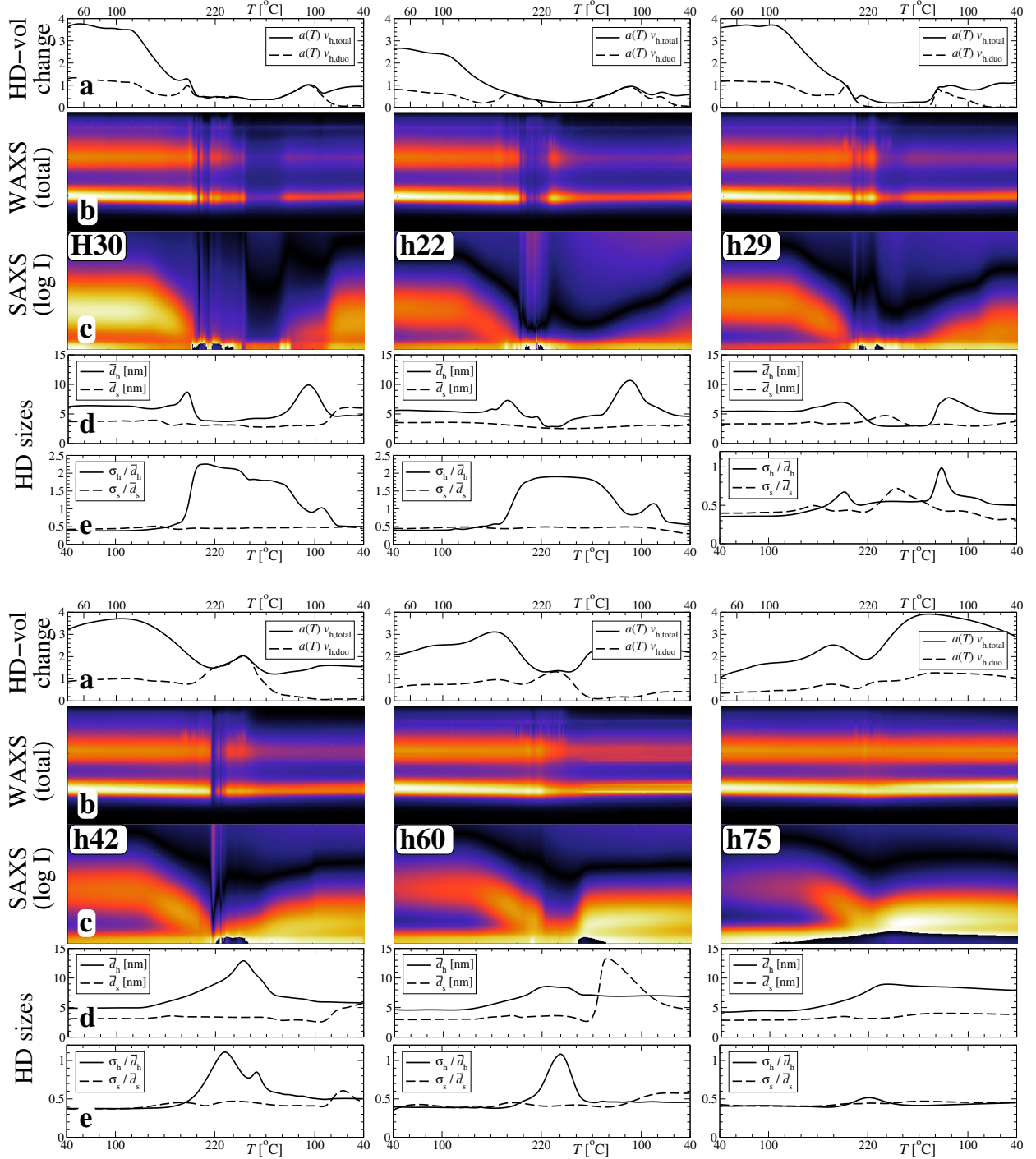


Figure 1: Melting and solidification of TPUs with varying hard segment content (HSC) as a function of processing temperature. Samples are heated and cooled with $|\dot{T}| = 20 \text{ K/min}$, $T_{max} = 220 \text{ }^\circ\text{C}$, 15 s dwell-time at T_{max} . Presented are scattering data and results of morphology analysis. **H30**: Hot processing, HSC = 30 wt%. — Cooler processing: **h22**, **h29**, **h42**, **h60**, **h75**. Numbers indicate the HSC. **a**: volume fractions of hard domains. **b**: Total WAXS intensity curves $I_{W,total}(s)$, $1 < s < 8 \text{ nm}^{-1}$. **c**: SAXS $\log(I(s))$, $0 < s < 0.25 \text{ nm}^{-1}$. **d**: average domain diameters. **e**: widths of the domain-size distributions characterized by their relative standard deviations (Subfigure **H30** from previous work [11])

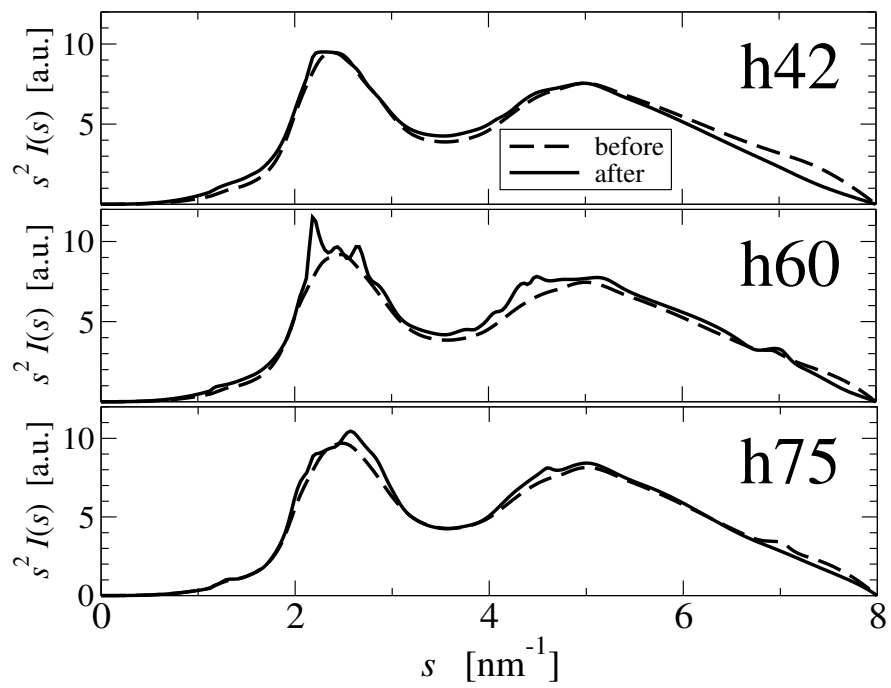


Figure 2: Before and after the temperature cycle. Comparison of the curve shapes of the total WAXS intensities, $s^2 I(s)$, for the materials with $\text{HSC} \geq 42$ wt%. Dashed lines: neat materials. Solid lines: After the temperature treatment. HSC is the numerical part of the label.

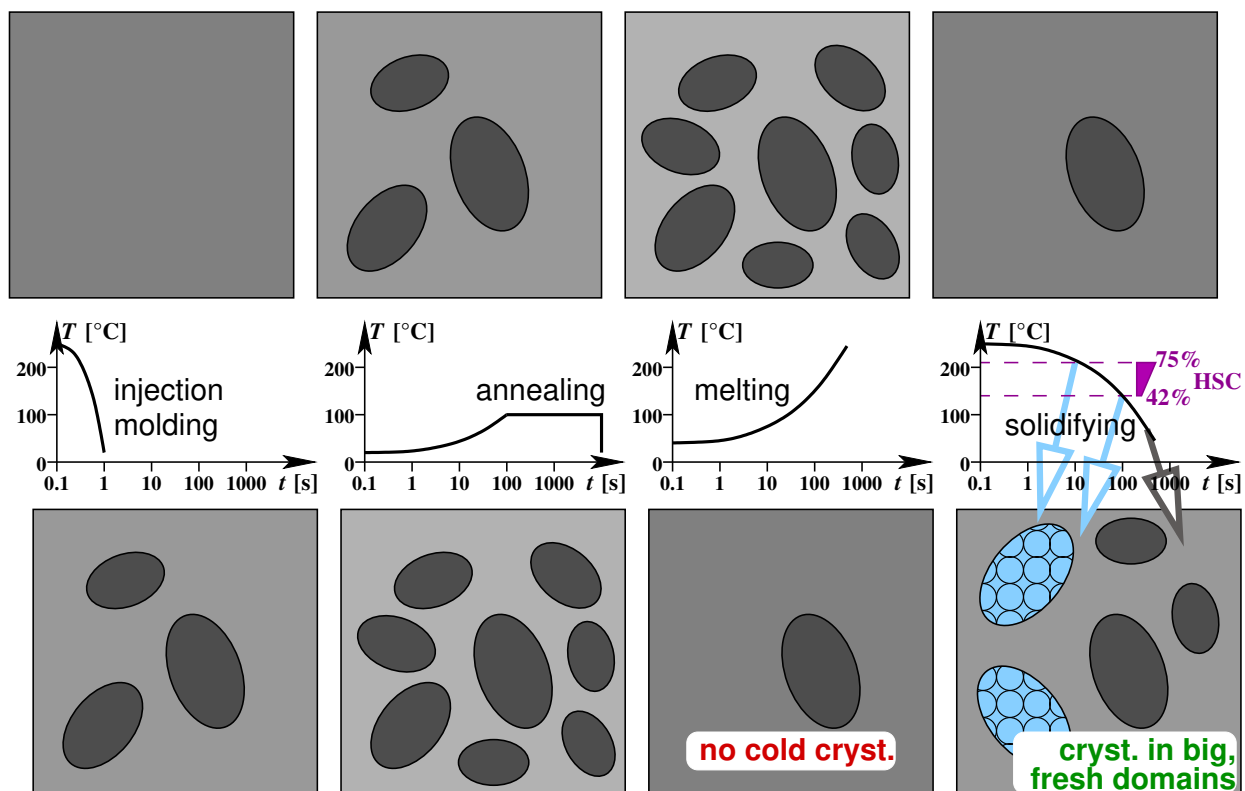


Figure 3: The dominant effects of hard-domain evolution and crystallization at the thermal processing steps of crystallizable TPU materials from the present investigation. Segregation processes within the colloidal melt are not sketched

List of Tables

1 Comparison of the positions of the main peaks in h60 with crystallographic studies on single crystals from MDI/BD [9,44]. Miller indexing (hkl) according to Born et al. [9] 22

Table 1: Comparison of the positions of the main peaks in h60 with crystallographic studies on single crystals from MDI/BD [9, 44]. Miller indexing (hkl) according to Born et al. [9]

h60		single crystal	
$s_{m,obs}$ [nm^{-1}]	d_{obs} [\AA]	d_{th} [\AA]	hkl
2.19	4.6	4.77	$\bar{1}04$
2.44	4.1	4.27	011
2.65	3.8	3.90	012